Bubble formation in nanopores: a matter of hydrophobicity, geometry, and size

Alberto Giacomello & Roland Roth

Published online: 27 Sep 2020.

Submit your article to this journal

View related articles

View Crossmark data

Taylor & Francis
Taylor & Francis Group

REVIEW

OPEN ACCESS Check for updates

Bubble formation in nanopores: a matter of hydrophobicity, geometry, and size

Alberto Giacomello [a] and Roland Roth [b]

aDipartimento di Ingegneria Meccanica e Aerospaziale, Sapienza Università Di Roma, Rome, Italy;
bInstitut Für Theoretische Physik, Eberhard Karls Universität Tübingen, Tübingen, Germany

ABSTRACT

This review focuses on the phase behaviour of liquids in nanoscale confinement, which promotes drying by a combination of hydrophobicity, small size, and high degree of confinement. In these conditions, the vapour phase can form at exceptionally large pressures or low temperatures as compared to bulk vaporisation, giving rise to the unexpected formation of bubbles. A general framework is introduced which allows to understand the main effects of confinement on the thermodynamics and on the kinetics of drying. The relevance of such phenomena is discussed in the realm of biological nanopores, specifically ion channels, and in nanoporous materials. The emergence of nanoscale effects not accounted for in macroscopic theories is discussed together with the open challenges in this rapidly expanding field.
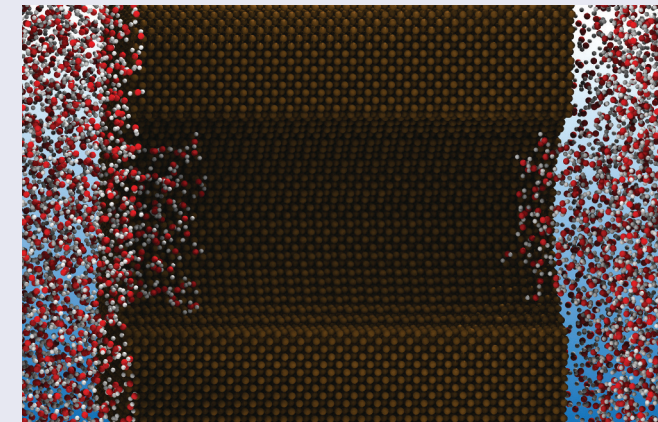
CONTACT Alberto Giacomello alberto.giacomello@uniroma1.it Dipartimento di Ingegneria Meccanica e Aerospaziale, Sapienza Università di Roma, Via Eudossiana 18, 00184 Rome, Italy Roland Roth, Institut für Theoretische Physik, Eberhard Karls Universität Tübingen, Auf der Morgenstelle 14, D - 72076 Tübingen, Germany; Roland Roth roland.roth@uni-tuebingen.de Institut Für Theoretische Physik, Eberhard Karls Universität Tübingen, Auf der Morgenstelle 14, Tübingen, Germany

1. Introduction

The energetic cost of forming a vapour bubble inside pure liquid bulk water at ambient conditions is so large that this process is effectively precluded. However, this process routinely occurs and plays a crucial role in a number of fields including engineering, biology, and material science. What is the origin of this seeming conundrum? In this review we discuss how drying, i.e. the formation of a vapour phase starting from the liquid one, can be dramatically favoured by nanoscale confinement; in particular, we focus on liquids in nanopores. We show that drying crucially depends on the hydrophobicity, on the geometry, and on the characteristic size of the confinement. Such effects are of central relevance for a wealth of biological phenomena which naturally occur at the nanoscale and for a number of engineering and nanotechnology applications.

It has been long known that the presence of impurities can dramatically expedite the formation of vapour bubbles, for instance, giving rise to cavitation – a dangerous phenomenon in many engineering applications [1,2]. Such impurities may be small particles present in the fluid or extended surfaces with asperities and/or chemical heterogeneities [3]. Recently, research has focused on what happens when the characteristic size or distance of solid surfaces are of nanometre size or less, i.e. when confinement is extreme. In these conditions, the liquid between two hydrophobic surfaces can undergo drying, causing an attractive force between them. In biology, this gives rise to the so-called hydrophobic effect in which two hydrophobic particles attract at long range, up to few nanometres [4–7]; this effect plays an important role in protein folding [8], molecular recognition [9], and, more in general, in protein and membrane assembly [10,11]. Fundamental studies have considered the phase behaviour of liquids in confinement finding that drying can be significantly favoured in nanoscale enclosures [12–17]. In particular, recent works tried to explain in terms of line tension the modified drying rates measured in theory [18], simulations [19–21], or experiments [22]. In technology, nanoscale confinement has been recently proposed as a means to create superhydrophobic surfaces capable of passively restoring the 'dry' superhydrophobic state after wetting has occurred [23–27].

The case of nanopores on which this short review is focused is particularly relevant in biology, as hundreds of different transmembrane proteins have this approximate shape and are often hydrophobic. An important example is that of ion channels, which constitute the gates of cells, through which the selective transport of ions across the hydrophobic cellular membrane occurs [28]; given that these channels have characteristic size ranging from 2 to a fraction of a nanometre and are typically hydrophobic, complete drying of the pore may occur interrupting the ionic current – this gating

mechanism is known under the name of hydrophobic or 'bubble' gating [29–36].[1] Other examples of biological hydrophobic nanopores in which drying may occur include lipids ion channels [37,38] and other biological channels engineered for nanopore sensing [39–41].

Drying may also occur in non-biological nanopores; an important example is hydrophobic nanoporous materials: when immersed in liquid water, due to the extreme confinement, drying within the pores can occur at pressures as large as tens of megapascals [22,42]. Wetting of these pores occurs at pressures which are larger than (or, in some cases, equal to) the drying one [43,44]. The value of the wetting and drying pressures depends on the geometry, chemistry, and size of the material [21,45]. Exploiting wetting/drying cycles, systems composed of a liquid and a lyophobic nanoporous material – the so-called heterogeneous lyophobic systems (HLS) – have been proposed in various technological applications, because of their ability to store mechanical energy in the form of surface energy [21,45–48]. When the wetting and drying pressures are much different, HLS can instead be used to damp energy, e.g. mechanical vibrations [49–51]. Furthermore, drying in nanopores is central in a number of nanotechnological applications including nanofluidics [52], nanopipettes [53], solid-state nanopores for sensing [54,55], engineering nanopores capable of gating [56,57], nanopore membranes [58,59], including for water desalination [60,61], nanofluidic channels [62], and carbon nanotubes [63].

Experiments on drying of nanoscale cavities are complex, due to the difficulty of concurrently characterising the cavity geometry, its surface characteristics, and its wetting state. More fundamentally, at the nanometre scale, the scale separation between the confining surfaces and liquid particles decreases and careful definitions of surfaces and volumes are needed in order to be able to interpret experiments. In this context, the synergy of experiments, theory, and simulation becomes a necessity, because, as discussed in this review, these tools provide complementary pieces of information needed in order to construct a picture of the phase behaviour of nanoconfined fluids. Checco et al. [64] used small-angle X-ray scattering in order to characterise the wetting of superhydrophobic surfaces upon varying pressure; the characteristic dimensions of the regular textures were of tens of nanometers and only partial drying was observed in some textures. In order to investigate drying in even smaller confines, monodisperse nanoporous materials proved a more convenient system, as the measurement can be done on an ensemble of pores [42,65]. Such benchmark systems will be considered in some detail because they allow to test the limits of available theories at the nanoscale. In the case of biological nanopores, the experimental difficulty is further enhanced by the structural and chemical complexity of such soft confines. Recently, high-resolution structures of ion channels have been resolved [66], which suggest that drying is

indeed possible in such conditions, but cannot provide a direct evidence. On the other hand, electrophysiology allows to verify indirectly and on a larger scale the blocking of pores by bubbles, by measuring the ionic current through single and multiple ion channels [67]. Electrophysiology techniques also allow to record the duration and kinetics of pore-blocking events, which typically give rise to a random telegraph signal in single-channel measurements [68]. Similar techniques are also routinely applied to identify drying of synthetic nanopores [57,58]. In between structural studies and electrophysiology, atomistic simulations play an important role [69], because they allow to link the structure with the microscopic mechanisms giving rise to function – here specifically hydrophobic gating.

Having briefly recapitulated the importance of drying in nanopores in biology and technology, we now sketch the plan of this review. In Sec. 2.1, we introduce the main concepts necessary to build a theory of drying in confinement and obtain the coexistence conditions for the confined vapour and liquid phases in geometries of increasing complexity. We borrow many results obtained for capillary condensation [70–74], which is concerned with the opposite problem of formation of a liquid phase from the vapour, aided by the presence of nanopores. In Sec. 2.2, the classical nucleation theory of drying in confinement is introduced, which allows to describe the kinetics of bubble formation in nanopores. Nanoscale corrections to this macroscopic theory are then discussed in the light of available simulations and experiments. The final section is dedicated to draw conclusions and to illustrate open problems in the field.

2. Theory of nanoconfined drying

2.1. Thermodynamics of drying

We start by considering a fluid in the grand canonical ensemble[2] that is in contact with a smooth planar wall. The free energy of this system is given by

$$\Omega_{wall} = -PV + \gamma A, \tag{1}$$

where P is the bulk pressure of the fluid, γ the surface tension of the fluid at the wall, and V and A are the volume of the system and the surface area of the wall. Note that while Ω and P are well defined and unique, the volume V depends on the separation of the system from the wall and has to be defined. As a consequence also γ, the surface tension of the system at a wall depends on this definition. This is not a problem, because γ cannot be measured experimentally and hence a definition-dependent wall surface tension does not lead to any inconsistencies.

If the fluid can separate into a liquid (l) and a vapour (v) phase, at coexistence one can observe a drop with Young's contact angle θ_Y at the

wall. If the (macroscopic) contact angle of the wall is smaller than 90° one considers the surface to be solvophilic or hydrophilic, in the case of water. The contact angle depends in general on temperature and small values of θ_Y are possible. In the case of $\theta_Y \rightarrow 0$ one speaks of complete wetting of the surface by the liquid [71]. In contrast, if $\theta_Y > 90°$ the surface is considered to be solvo- or hydrophobic. On smooth surfaces, contact angles $\theta_Y > 120°$ are not observed, at least with water, because the attraction between atoms of the surface and of the fluid does not vanish, it is only weaker than the fluid-fluid attraction. In computer models, one can easily realise perfect hard walls, without attraction, and observe contact angles of up to 180°. In a real system, large values of θ_Y the (apparent) contact angle can be observed at geometrically structured (atomically rough) walls [75,76].

The contact angle θ_Y is related to the solid-vapour surface tension γ_{sv}, to the solid-liquid surface tension γ_{sl}, both of which depend on the definition of the system volume, and to the surface tension of the free liquid–vapour interface γ_{lv} through Young's equation

$$\cos \theta_Y = \frac{\gamma_{sv} - \gamma_{sl}}{\gamma_{lv}}, \tag{2}$$

where the geometry dependency of γ_{si}, $i = l, v$ cancels out and results in a well-defined contact angle.

In a slit pore consisting of two parallel, planar, and equivalent walls separated by a fixed distance $L \gg \xi$, where ξ is the bulk correlation length, the free energy of the confined fluid, to a good approximation, is given by [70,77]

$$\Omega_{slit} = -PV + 2\gamma A = A(-PL + 2\gamma), \tag{3}$$

where the factor 2 in the surface term compared to Equation (1) accounts for the presence of two walls; we have made use of $V = AL$. Clearly, if L becomes comparable to ξ correlation effects will make this approximation less accurate.

At bulk coexistence, i.e. assuming thermal ($T_v = T_l$), chemical ($\mu_v = \mu_l$), and mechanical ($P_v = P_l$) equilibrium between a vapour and a liquid phase, the only difference between the confined phases is due to the surface term and it follows that in a solvo/hydrophilic slit the liquid phase is stable, because $\gamma_{sl} < \gamma_{sv}$ and in a solvo/hydrophobic slit the vapour phase is the preferred one, as $\gamma_{sl} > \gamma_{sv}$. If the fluid is off but close to bulk coexistence a vapour and a liquid phase in the slit can coexist at the same temperature and chemical potential if they possess the same free energy ($\Omega_v = \Omega_l$). From this assumption of coexistence in the slit geometry one can define the pressure difference $\Delta P = (P_l - P_v)$ required for the transition

$$\Delta P = -\frac{2(\gamma_{sv} - \gamma_{sl})}{L} = -\frac{2\gamma_{lv}\cos\theta_Y}{L}, \qquad (4)$$

where we have made use of Young's equation at the wall, (2), in order to convert the difference in the surface tensions into that of the free interface times the cosine of the contact angle. This equation is called Kelvin equation. Note that the capillary condensation or evaporation predicted by the Kelvin equation can be first order with hysteresis effects, if the temperature is below the *capillary* critical point, or continuous if it is above [77]. Close to coexistence, where the chemical potential is given by $\mu_i = \mu_{co} + \delta\mu$, $i = v, l$, with μ_{co} its value at coexistence, and $\delta\mu$ a (small) deviation, it is possible to expand the pressure in a Taylor series: $P_i = P_{co} + (\partial P_i/\partial\mu)_{T,V}\delta\mu + \mathcal{O}(\delta\mu^2) = P_{co} + \rho_i\delta\mu + \mathcal{O}(\delta\mu^2)$, where the Gibbs-Duhem relation was employed and ρ_i denote the coexisting bulk densities. This leads to the expression $\Delta P = \Delta\rho\delta\mu + \mathcal{O}(\delta\mu^2)$ with $\Delta\rho = \rho_l - \rho_v$, which is often used in theoretical studies.

Taking into account that $\gamma_{lv}/L > 0$, there are two different scenarios for which Equation (4) has physically meaningful solutions: (i) If one considers a stable liquid phase, i.e. $P_l > P_v$ or $\Delta P > 0$, one finds a physical solution for $\cos\theta_Y < 0$, i.e. if $\theta_Y > 90°$, meaning if the slit is solvo/hydrophobic. In that case one can observe capillary evaporation – often also referred to as drying – of the slit pore. (ii) If one starts with a stable vapour phase with $P_v > P_l$ or $\Delta P < 0$, a physically meaningful solution of Equation (4) requires $\cos\theta_Y > 0$ or $\theta_Y < 90°$, i.e. a solvo/hydrophilic slit. In this case, the transition from the vapour to liquid phase is called capillary condensation.

While the treatment of the infinite slit pore is instructive and contains the essential physics of capillary condensation and evaporation, the theory employed so far is not suitable for strongly confined fluids, which are important in many applications. To allow for narrow pores we make use of the morphometric thermodynamics [78] that employs the ansatz that the free energy of a confined fluid can be written in terms of four geometrical terms

$$\Omega_{morph} = -PV + \gamma A + \kappa C + \bar{\kappa}X \qquad (5)$$

where C and X are the integrated (over the surface area) mean and Gaussian curvature of the confining space, respectively, and κ and $\bar{\kappa}$ are the corresponding free energy costs to bend the solid–fluid interface. If one imagines a configuration of fluid particles close to a wall it becomes intuitively clear that the interaction energy depends on the shape of the solid wall and hence on its curvature because the interaction between a fluid particle with another fluid particle differs from that with a particle from the solid. By averaging over all fluid configurations the shape or curvature dependence is picked up by the free energy. This morphometric ansatz extends the form of

Equation (3) by two curvature terms. The rationale behind the morpho-
metric ansatz is that the free energy of a system in the thermodynamic limit
is extensive and can be written as a sum of products of pairs in the form of
a geometrical measure (e.g. V and A) that is extensive times an intensive
thermodynamical coefficient that does not depend on the shape of the
system. The morphometric free energy is the most general extensive form
in $d = 3$ for a single-phase/single-species system, because there are exactly
$d + 1$ linearly independent extensive geometrical measures in d dimensions
[79] and V, A, C, and X are linearly independent.

In order to illustrate the concept, we consider a part of length L of an
infinite cylinder (in order to avoid end effects) with fixed radius R_c. The
volume $V_c = R_c^2 \pi L$ and the surface area $A_c = 2\pi R_c L$ are straightforward to
calculate. For the integrated curvatures, we first note that a surface in $d = 3$
has, at any given point, two principal radii of curvature, denoted by R_I and
R_{II} from which one can compute the local mean curvature $H = (1/R_I +
1/R_{II})/2$ and the local Gaussian curvature $K = (1/R_I)(1/R_{II})$. For the
cylinder we consider here, the two principal radii of curvature are constant
on the entire surface: $R_I = \pm R_c$, depending on whether we consider the
curvature of the outside face where $R_I = +R_c$ or of the inside face where
$R_I = -R_c$, and $R_{II} = \infty$. From this, it is easy to see that $H = \pm 1/(2R_c)$ is
constant and $K = 0$. It follows directly that the mean curvature integrated
over the surface of the cylinder is given by

$$C = \int dA H_c = H_c \int dA = H_c A_c = \pm L\pi. \tag{6}$$

Similarly, X is the surface integral of K, which vanishes for the cylinder.
Here we are mainly interested in a fluid confined inside a cylindrical pore,
for which the free energy for a pure phase i within the morphometric
approach is given by [78,80]

$$\Omega_{c,i} = -P_i R_c^2 \pi L + \gamma_i 2\pi R_c L - \kappa_i L\pi, \quad i = l, v. \tag{7}$$

From this, we can easily generalise the Kelvin equation, Equation (4), for the
slit to the cylindrical geometry by demanding (i) thermal and (ii) chemical
equilibrium and (iii) equal free energies of the coexisting phases [80]. This
results in an equation that can be solved for ΔP:

$$\Delta P = -\frac{2\gamma_{lv} \cos\theta_Y}{R_c} - \frac{\Delta\kappa}{R_c^2} \tag{8}$$

where $\Delta\kappa = \kappa_l - \kappa_v$. It is important to note here that while ΔP and hence the
complete expression on the r.h.s. of Equation (8) is an observable, i.e. it can
be measured experimentally, the individual terms on the r.h.s. of Equation
(8) depend on the choice of the dividing interface. In DFT calculations of

a square-well fluid in a hydrophobic cylindrical pore [80] $\Delta\kappa$ was found to be positive.

In order to illustrate the effects of confined drying in the biological context, we briefly discuss the mechanism of hydrophobic or bubble gating of ion channels [30,32,34–36]. The geometry of the voltage gate potassium channel KcsA [66] is known to change in the gate region in response to a change of the membrane potential. The gate geometry employed in DFT studies [32,81,82] follows the model of Ref [83] and is depicted in Figure 1. In a simplified manner, the geometry of the gate can be represented by a part of a cone that has a fixed height, one (upper) fixed diameter and one (lower) varying diameter, denoted by D in Figure 1. If D is sufficiently wide compared to the diameter of water, which is set at 2.8 Å in this calculation [32], the channel is considered open for ions to diffuse through the channel along their electro-chemical gradient. In that case, the slightly hydrophobic gate is assumed to be filled for most of the time with water, as shown on the right side of Figure 1. When the channel is open the probability of finding a bubble in the gate, $P_{bubble}(D)$ is close to zero, i.e. most of the time a constant current of ions can be measured in a patch-clamp experiment
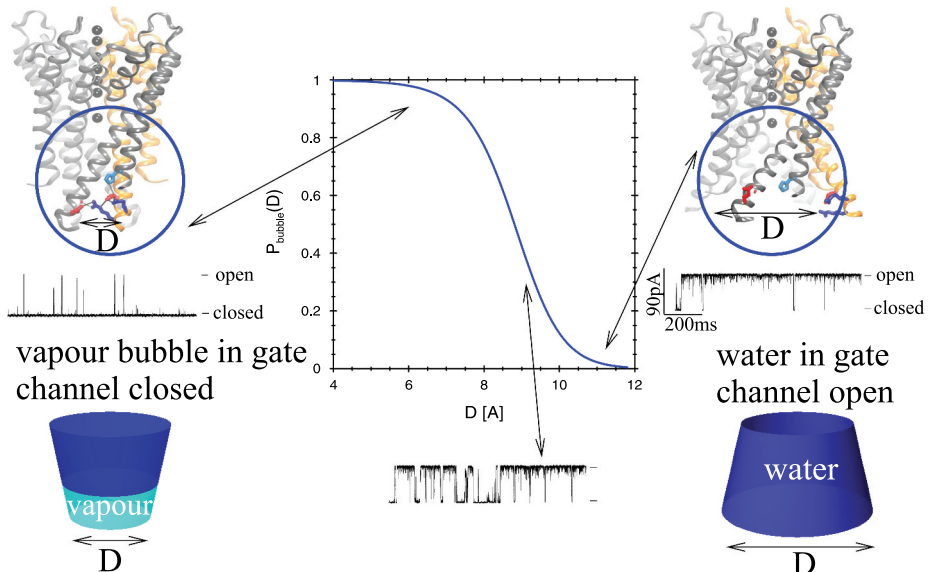
Figure 1. The probability $P_{bubble}(D)$ of finding a bubble in a slightly hydrophobic gate of a biological ion channel following the geometry of KcsA [66] as a function of the lower diameter D, which should be compared to the diameter of water that is set at 2.8 Å in this calculation [32]. As the lower diameter D changes from narrow to wide, the probability of finding a bubble changes from roughly 1 to nearly 0. The key quantity driving this behaviour is $\Delta\Omega$, given in Equation (9), the difference in the free energy of the gate blocked by a bubble and one in the same geometrical configuration filled by water. The KcsA structures are adapted from Ref [83], Copyright (2008) National Academy of Sciences, U.S.A. The ion currents shown in this figure illustrate the result that can be observed in patch-clamp experiments [68].

[68]. As the lower diameter D of the gate is reduced, the chance of finding a bubble in the gate is increased, which results in an increased $P_{bubble}(D)$. This in turn gives rise to an ion current switching on and off, resembling a random telegraph signal at intermediate values of D. For sufficiently small values of D the probability of finding a bubble in the hydrophobic gate approaches 1, as illustrated on the left side of Figure 1 and the ion current vanishes almost all the time. It is interesting to note that the shape of the ion current and the time scales observed in patch-clamp experiments can only be explained if the channel switches between bistable states, i.e. two states that correspond to almost equal (local) free energy minima that are separated by a free-energy barrier. This scenario follows naturally from the bubble gating model.

Employing the morphometric approach [78] it is straightforward to make an ansatz for the free energy of the gate filled with water or blocked by a bubble [32]. When the gate is approximated by a two-state model, where the gate is either filled with water with a free energy Ω_{water} and hence open for ion diffusion, or blocked by a bubble with a free energy Ω_{bubble} and hence closed for ion diffusion, the probability of finding a bubble in the gate depends on

$$\begin{aligned} \Delta\Omega(D) &= \Omega_{bubble}(D) - \Omega_{water}(D) \\ &= \Delta P V_\nu + \Delta\gamma A_\nu + \Delta\kappa C_\nu + \gamma_{lv}(A_{lv,1} + A_{lv,2}), \end{aligned} \quad (9)$$

where V_ν, A_ν, and C_ν are the geometrical measures (volume, surface area, and mean curvature integrated over the surface area) of the part of the gate that is filled by the vapour phase. In addition, one finds two liquid–vapour interfaces with surface area $A_{lv,1}$ and $A_{lv,2}$. Effects due to line tensions [84,85] at the liquid-vapour-protein contact line are neglected. In the two-state model [32] it follows that the probability of finding a bubble is given by

$$P_{bubble}(D) = \frac{1}{1 + \exp(\beta\Delta\Omega(D))}, \quad (10)$$

with $\beta = 1/(k_B T)$, where k_B is the Boltzmann constant and T is the temperature.

The two-state model above, which takes for the bubble only the most likely geometry into account, is rough and can be refined by performing a partition sum over all possible bubble geometries [81]. However, the two-state model captures the essential physics as was verified by a $3d$ DFT calculation [82]. In this calculation, the channel geometry is represented by a three-dimensional external potential $V_{ext}(\mathbf{r})$ that acts on water, modelled by a square-well fluid. In the narrow geometry, shown in Figure 2(a), the hydrophobic gate is blocked by a bubble, while it is filled by water in a wider geometry, depicted in Figure 2(b). As the structure of water, or the

square-well fluid, is determined by freely minimising the density functional, it is possible to obtain ensemble-averaged density profiles $\rho(\mathbf{r})$ of the fluid in the channel. From these profiles, it becomes clear that the idea of a simple bubble shape and a clearly defined and sharp liquid–vapour interface is not valid for ensemble-averaged bubble shapes and interfaces on these small length scales, but the main physics is still covered surprisingly well by the previously mentioned two-state model of the gate.

2.2. Kinetics of drying

The coexistence conditions derived above clearly show the effect of confinement on the phase behaviour of fluids; in addition, a prediction is made on what is the stable phase at given conditions, i.e. that having minimal free energy, and on the relative stability of possible metastable states, i.e. the free energy difference between two states. The predicted equilibrium is reached *in the thermodynamic limit*, i.e. for infinite equilibration times. However, one may still wonder what is the characteristic time scale to form the stable phase starting from the metastable one – the kinetics of the transition: in actual experiments, the metastable phase may be so long-lived that the transition is never observed; in some bistable systems, instead, the kinetics may be fast enough to observe frequent switching between the states. In addition, in order to understand the hysteresis phenomena often encountered in wetting and drying processes, it is crucial to discuss the metastabilities involved. In the following, by leveraging classical nucleation theory, it will be shown that confinement not only modifies the coexistence conditions of liquid and vapour, but also the kinetics of formation of the new phase.
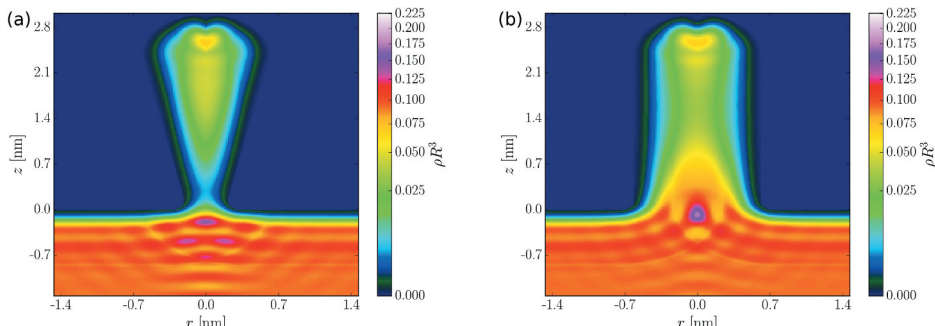
Figure 2. The ensemble averaged density profile $\rho(\mathbf{r})$ of water, modelled as a square-well fluid, in two geometrical configurations of an ion channel following the geometry of KcsA [66] treated by a 3*d* DFT calculation. In the narrow gate geometry a bubble forms in the gate and blocks ions from diffusing through the channel, while a sufficiently wide gate allows water in the gate that, in turn, enables ions to follow their electro-chemical gradient. Figures are adapted from Ref [82].

2.2.1. Classical nucleation theory

We consider here, without loss of generality, classical nucleation theory (CNT) in the case in which a stable vapour phase nucleates from a metastable liquid phase. In the simplest case of homogeneous nucleation, a domain of the new phase is formed in the bulk of the metastable liquid driven by the free-energy difference per unit volume of the two phases, $\Delta P < 0$. On the other hand, the new domain grows at the expense of forming a liquid–vapour interface, whose free-energy cost per unit area is given by the surface tension γ_{lv}. In order to minimise the surface cost, homogeneous nucleation typically happens via the formation of a spherical domain – a bubble – whose radius progressively grows. The competition of favourable bulk terms and unfavourable surface terms is won by former when the bubble exceeds a certain size, called the critical nucleus. This critical bubble is connected to a maximum in the free-energy, which defines a free-energy barrier $\Delta\Omega^{\dagger} = \Omega_{max} - \Omega_{min}$ which needs to be overcome in order to form the new phase (Figure 3(a)); this scenario is common to all nucleation phenomena. As will be shown in Sec. 2.2.2, the critical volume is crucial in determining the dependence of the kinetics on the pressure (or the extrusion pressure in fixed-frequency experiments), with lower (respectively, higher) sensitivities corresponding to lower critical volumes.

Thermal motion of the atoms continuously perturbs the system close to the free-energy minimum in which it is stuck. The kinetics of formation of a bubble, or the opposite case of condensation of a drop, is governed by the time one has to wait in order to observe a thermally driven fluctuation capable of overcoming the free-energy barrier. Since large fluctuations are improbable, this time t increases exponentially with the free-energy barrier $\Delta\Omega^{\dagger}$ measured in thermal units $k_B T$ [86,87]:
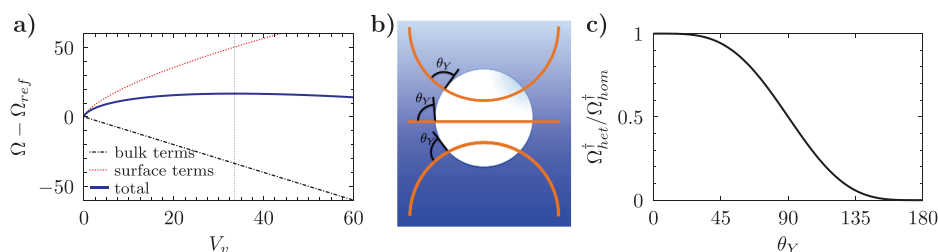
Figure 3. Illustration of classical nucleation theory (CNT). a) Total free energy for homogeneous nucleation (solid blue line), given by the sum of energetically favourable bulk terms (dash-dotted line) and unfavourable surface ones (dotted line). b) Comparison of critical bubbles for heterogeneous nucleation at surfaces with simple shapes highlights the influence of surface curvature on the critical volume and, consequently, on the free-energy barriers (adapted from [89], see also [86]). c) Ratio of the nucleation free-energy barrier at a flat surface and the bulk barrier as a function of the contact angle θ_Y of the surface.

$$t = t_0 \exp\left(\frac{\Delta\Omega^\dagger}{k_B T}\right). \tag{11}$$

In Equation (11), t_0 is the prefactor which sets the timescale of the phenomenon when the barrier is small. The kinetics described by Equation (11) is typical of rare events, i.e. those processes characterised by a long timescale t necessary to observe an improbable, large thermal fluctuation and a short timescale of the transition itself, which happens readily once triggered by a suitable fluctuation. This disparity poses an inherent difficulty in observing nucleation events in both experiments and simulations. Given the exponential dependence of t in Equation (11) on the free-energy barriers, nucleation events become frequent enough to be observed only when barriers are at most 1 order of magnitude larger than the thermal energy $k_B T$. In Sec. 2.2.2 it will be shown that this is indeed the case for drying/wetting in nanoscale confinement.

Following Ref [88], a simple calculation based on Equation (11) shows that at 20°C the vapour phase can nucleate from bulk liquid water only for very large negative deviations from coexistence, $\delta\mu \ll 0$, corresponding to a tensile state of the liquid with negative pressures $P_l = -168$ MPa. In such conditions, the critical bubble has the size of approximately 1 nanometre. So why do bubbles actually form in water even at ambient conditions, and, in particular, in nanopores? What is specific to confined drying? The answer is that the presence of confining solid surfaces or surface asperities can dramatically change (the thermodynamics and) the nucleation kinetics as compared to the bulk case, by introducing two interfaces in competition – the solid-vapour and the solid-liquid – characterised by the free-energy costs γ_{sv} and γ_{sl}, respectively. In order to rationalise the role of solid surfaces on drying, starting from Equation (1), we express the free energy of a two-phase system in contact with a wall as:

$$\Omega = -P_l V_l - P_v V_v + \gamma_{lv} A_{lv} + \gamma_{sv} A_{sv} + \gamma_{sl} A_{sl}, \text{ or} \tag{12a}$$

$$\Omega - \Omega_{ref} = \Delta P V_v + \gamma_{lv}(A_{lv} + \cos\theta_Y A_{sv}), \tag{12b}$$

where the subscripts l, v, and s have been used to denote the liquid, vapour, and solid phases, respectively, and the related interfaces. One can further recall that the total volume of the system and the total surface area of the solid are constant, i.e. $V_l = V_{tot} - V_v$ and $A_{sl} = A_{tot} - A_{sv}$, respectively; this position, together with Young's equation (2), allows for the expression (12b), which groups together the constant terms in $\Omega_{ref} = -P_l V_{tot} + \gamma_{sl} A_{tot}$, which is the reference free energy of the confined liquid. This is a more expressive form of the free energy in that it makes explicit the competition between the liquid-vapour term, which is

always positive, and a second surface term related to the solid, which can have either positive or negative sign, in the hydrophilic ($\theta_Y < 90°$) and in the hydrophobic case ($\theta_Y > 90°$), respectively. As discussed in Sec. 2.1, the presence of hydrophobic walls changes the coexistence conditions, favouring the dry state.

We now focus on the effect of a solid surface on the *kinetics* of nucleation. CNT prescribes that, during nucleation, the relevant bubble is that mini-mising the free energy in Equation (12b) *constrained* to the current advancement of the process V_v [89,90]. In other words, in the quasi-static limit, the bubble shape having maximum probability is determined solely by the surface energy terms [89,91]. Because of the additional surface terms in Equation (12b), in which the energetic cost of the liquid–vapour interface γ_{lv} is multiplied by a factor $|\cos \theta_Y| \leq 1$, the critical heterogeneous bubble can have a free energy significantly lower than the spherical homogeneous bubble, by assuming different shapes, which encompass interfaces with lower energetic cost (Figure 3(b)). Interestingly, both hydrophilic and hydrophobic surfaces decrease the free-energy barriers; this can be quanti-fied, for instance, in the case of a flat surface with a prescribed contact angle θ_Y by considering the ratio between the heterogeneous and the homoge-neous drying barriers $\psi \equiv \Delta\Omega^\dagger_{het}/\Delta\Omega^\dagger_{hom} = (1 + \cos \theta_Y)^2(2 - \cos \theta_Y)/4$ (Figure 3(c)): the higher the contact angle, i.e. the more hydrophobic the surface, the lower the barriers for drying. The curvature of the confining surfaces can further change the shape of the critical bubble and thus affect the barriers [86]; these will increase in the case of a convex surface and decrease in the case of a concave one (Figure 3(b)). In all cases, by decreas-ing the free-energy barriers, the kinetics of heterogeneous nucleation accel-erates exponentially as per Equation (11). This discussion clarifies why the role of *heterogenous* nucleation, i.e. occurring at solid surfaces, is so impor-tant; it is by now accepted that cavitation in flows of engineering interest occurs mainly at impurities, known as nuclei [2,3,88]; indeed, only by extremely careful experiments excluding all sorts of contamination, it is possible to observe bulk nucleation in water [92,93].

It is interesting to remark that the presence of gases dissolved in the liquid, in particular hydrophobic ones, also plays an important role in facilitating bubble nucleation. In macroscopic bubbles the main effect is that of adding to the vapour pressure the gas one, thus shifting the equili-brium conditions towards the dry state [91]. This is known to play a role in cavitation nuclei entrapped in crevices [94]. In general, gases also change the other thermodynamic coefficients in Equation (9) [32] (see also [14]) further favouring drying of nanopores. In ion channels, this corresponds to favour-ing the closed state, which may help explaining the anaesthetic action of some volatile general anaesthetics [32], which may reversibly cause gating of

some classes of channels. This gas-assisted drying mechanism may also be relevant for controlling drying in superhydrophobic surfaces, artificial nanopores, and in liquid chromatography columns [95, 96]. However, the kinetics of this process remains still unexplored at the nanoscale. The change of thermodynamic coefficients due to dissolved gases also has consequences on the existence and stability of surface nanobubbles [97].

Let us now focus on the case of drying in non-trivial confining geometries. Equation (12b) implies that the geometry of confinement is able to modify the shape of the nucleus of the new phase determining the proportions of A_{lv} and A_{sl} for a given V_v. In general, confining a liquid within a complex surface can modify the bubble morphologies along the entire nucleation process decreasing the free-energy barriers [26] and, sometimes, breaking the thermally activated process in multiple steps with lower barriers, i.e. acting as a catalyst for the nucleation of bubbles [91]. In particular, when the size of the confinement is comparable to that of the critical bubble, the drying kinetics can be dramatically affected, see, for example, [20,98]. For instance, special geometries such as a (sufficiently hydrophobic) conical crevice can favour the formation of a critical bubble which maximises the solid-vapour interface inside the crevice while keeping a small liquid-vapour area at its mouth, thus decreasing the free-energy barriers and accelerating drying [91]. In some conditions, the barriers may vanish altogether, giving rise to wedge drying [27,99,100] (or the opposite case of wedge filling [101]). It should be noted that in strong confinement the relevant system typically encompasses only a finite amount of matter, i.e. the confined fluid; in this sense, it is different from a classical phase transition in which an infinite bulk is involved. This also implies that the opposite 'wetting' transition, i.e. the process leading from the confined vapour to the confined liquid can happen with finite barriers, i.e. in finite times.

The case of drying in a nanoscale cylinder is particularly relevant for this review as this is perhaps the simplest example of a nanopore. Reference [42] reports experimental wetting and drying curves for water at ambient temperature in almost perfectly cylindrical hydrophobic nanopores (hydrophobised MCM-41) with radii varying, depending on the sample, approximately between 2 and 6 nm. The porous material is immersed in liquid water to form an HLS; the system is then subjected to pressure variations via a hydraulic press (Figure 4(a)). When starting from the confined liquid and progressively decreasing the pressure, drying (referred to as 'extrusion' in the specialised literature) of such pores occurs at very large pressures, up to 30 MPa, which indicates that the presence of hydrophobic walls, together with the nanoscale size of the confinement, renders liquid water metastable at unusually large pressures. On the other hand, when starting from the confined vapour and increasing the pressure, wetting ('intrusion') always occurs at pressures larger than the drying one, in the cited case 60 MPa. The
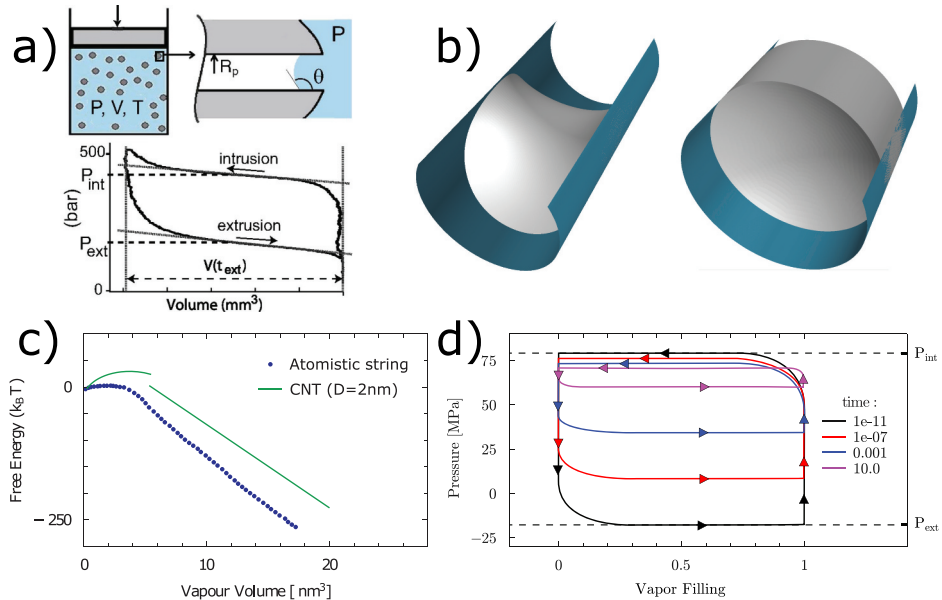
Figure 4. Drying process in a cylindrical nanopore: a) experimental results from [22]; b) bubble morphologies predicted by CNT; c) comparison of free energy from atomistic simulations (circles) and CNT (green line); d) drying/wetting cycles in cylindrical nanopores for different durations of the cycle. Panel a) is adapted from [22], panels b-d) from [21].

overall wetting/drying cycle displays a large hysteresis loop typical of strongly metastable systems (Figure 4(a)). The monodispersity of the porous material allowed the authors to relate the macroscopic characterisation of the wetting and drying processes of the macroscopic systems comprising hundreds of porous grains to the geometrical and chemical characteristics of a single pore. Thus, the conclusions drawn for an ensemble of pores shed light on the drying and wetting processes in extreme confinement, also in the case in which a single nanopore is of interest, e.g. in biological ion channels.

It worth mentioning that the strong hysteresis in the pressure cycles of Ref [42] implies that this type of HLS can be employed to dissipate energy [22], e.g. in dampers for mechanical vibrations. Other types of materials exhibit vanishingly small hysteresis and thus show promise for storing energy in the form of surface energy [102]. A third class of HLS exists in which, after liquid intrusion, no drying can be obtained simply by reducing the pressure to the ambient one; in this case, the typical application is in single-use 'bumpers' [46]. In general, these considerations underscore the importance of understanding the wetting and drying processes in nanoporous materials and of controlling them by designing the material properties, matching the liquid/solid pair, and tuning the operating conditions.

Reference [42] reports a CNT for drying in a cylindrical pore (see also [18]), which is useful to recall here. Results are obtained minimising the free energy in Equation (12b) for increasing values of the volume of the bubble confined in a cylindrical pore. The main theoretical finding is that the strongly confining cylindrical geometry forces the bubble to take two distinct morphologies along the nucleation process, depending on its progress: at the beginning of drying, the bubble is attached to the wall, breaking the axial symmetry of the pore; as the bubble size becomes comparable to the pore diameter, the bubble becomes axially symmetric, with spherical-cap menisci delimiting it on the two sides (Figure 4(b)). The first case is the most important for the kinetics of drying as it allows the formation of the first bubble and its growth to the critical size (Figure 4(c), first portion of the green line): it is a clear example in which the critical bubble size is dictated by the size of the confining surface. This dominance of confinement on the critical bubble is reflected in the fact that the drying critical volume and the related free-energy barrier are almost insensitive to changes in the external pressure [21,22], at variance with the bulk case in which both have a strong dependence on the pressure, $V_{c,hom} = 4/3\pi\gamma^3 |\Delta P|^{-3}$ and $\Delta\Omega_{hom}^{\dagger} = 16/3\pi\gamma^3 \Delta P^{-2}$, respectively, and with cases in which confinement is not as pronounced [91]. The axisymmetric bubble morphology, instead, is concerned with the further expansion of the bubble until complete drying of the pore is achieved; accordingly, the extension of the related free-energy branch depends on the length of the pore and not only on its diameter. This second case is relevant for determining the reverse, i.e. the wetting free-energy barrier (see the next section for a discussion of the different behaviour of wetting and drying barriers with pressure).

A recent study [45] has shown that, in addition to pore size and chemistry, also fine details of the pore morphology may be relevant for determining the drying conditions. In particular, experiments on two kinds of hydrophobised mesoporous silica of similar size (6 to 10 nm) showed no drying for the material characterised by approximately cylindrical, independent pores, and drying at $\Delta P \approx 2$ MPa for the material with interconnected pores. With the aid of theory and simulations, the authors showed that the internal surface of the pores – encompassing pore interconnections or nanometre roughness – may be responsible for decreasing the surface free energy connected with drying of the pores, thus allowing drying even at positive pressures. Actually, barrierless drying occurs within the smallest cavities decorating the pore walls, due to their reduced size (~1 nm), and triggers drying at the larger scale of the main pores [27,103]. Experiments were then repeated using mercury and different kinds of porous materials, which confirmed the role of a small number of nanometre-sized pores in determining the drying of the whole material.

This brief overview of CNT in confined environments illustrated the combined action of hydrophobicity and confining geometry in accelerating the drying kinetics. This is first of all crucial for understanding why cavitation occurs at all in flows of engineering interest, in which the presence of microscopic impurities catalyses the formation [3] and regeneration [104] of cavitation nuclei. At smaller scales, an important realm in which drying in hydrophobic confinement plays a crucial role is biology; there, strong attractive forces are known to originate from the drying of liquid water confined between hydrophobic residues of proteins; this 'hydrophobic effect' has a role in protein folding and molecular recognition among others [6,8,11]. In ion channels, water is confined in a pore with (sub)nanometre diameter; the displacement of some residues, which make the pore narrower and/or more hydrophobic, has been recognised to give rise to drying, which blocks the ionic currents – the so-called hydrophobic or bubble gating of ion channels [29–36]. In some cases, even weakly hydrophilic pores can give rise to drying, due to their curvature and extreme confinement, as described by Equation (8) [32,80]. The third realm in which confined drying plays a crucial role is that of hydrophobic nanoporous materials immersed in liquid water; due to the combination of extreme confinement and hydrophobicity, drying may occur even at large pressure. In the latter cases, nanoscale confines are an essential condition to observe drying; it is therefore of crucial importance to discuss whether effects characteristic of the nanoscale are able to change the nucleation scenario presented so far, which is based on the assumptions of macroscopic capillarity. In the next section, we discuss nanoscale effects not included in CNT with particular attention to line tension.

2.2.2. Beyond classical nucleation theory – nanoscale effects

One of the limits of classical nucleation theory is that, in confinement, discontinuous drying processes are obtained as a result of the minimisation of the free energy subject to the only constraint of the bubble volume [89]. For instance, for drying in a cylinder, no intermediate morphologies between the two mentioned in the previous section (Figure 4(b)) are found; this leads to a discontinuity in the path and in the free-energy profile (see Figure 4(c), green line and Ref [42]). Unfortunately, this deviation occurs exactly at the transition state, which is crucial for determining the drying kinetics. This artefact is known to be due to an insufficient order parameter used in CNT, i.e. the volume of the nucleating phase, here the bubble's [89]. Using more general order parameters, such as the density field [105], alleviates the problem [106]. In Refs [21,107], the string method in collective variables was used together with atomistic simulations in order to obtain the free-energy profile and the drying mechanism(s) using the density field as the order parameter. This approach allows both to go beyond

the discontinuous CNT and to gather insights into the nanoscale effects relevant for drying in such nanoscale confinement as discussed below.

It is important to remark that, at the nanoscale, the drying free-energy barriers are typically of the same order of magnitude of the thermal energy available to the system, i.e. $k_B T$. Indeed, in the absence of line tension, a drying free-energy barrier is expected to scale as by $\gamma_{lv} L^2$ [98], where L is the characteristic size of the confinement; on the scale of 1 nm, this yields barriers of 10 to 20 $k_B T$, depending on the value of γ_{lv}. Plugging such values in Equation (11) shows that, at this scale, thermally activated drying events may become observable on experimental timescales. This may be relevant for water conduction in carbon nanotubes [63] or, more generally, in nanoporous membranes [58,59]. Similarly, ionic currents in electrophysiology measurements may show random blockage due to thermally activated bubble gating events. This is indeed typical of single ion channels measurements [68], which show random telegraph signals characterised by very fast switching and on and off currents lasting tens of ms, as depicted in Figure 1. In order to explain the random telegraph signal by drying/wetting events, the wetting free-energy barrier should be of the same order of magnitude of the drying one, to allow for the reverse transition to be observed. Since $\Delta\Omega^{\dagger}_{wet} = \Delta\Omega^{\dagger}_{dry} + \Delta\Omega$, this is the case when the free-energy difference between the open and closed states, $\Delta\Omega$ defined in Equation (9), is smaller than the barriers; if, instead, $\Delta\Omega \gg \Delta\Omega^{\dagger}_{wet} > 0$ the drying transition is irreversible on the scale of the experiment and the ion channel would remain in the closed state.

The fact that the drying/wetting barriers in nanoconfinement are of the order of few to tens of $k_B T$ also accentuates the dependence of the experimental drying and wetting conditions on the timescale of the measurement. While this variability is in principle always present in metastable systems, only the size of nanopores makes such dependence measurable. In the thermodynamic limit, the system is allowed to equilibrate for an infinite time and always falls into the global minimum of the free energy, as described in Sec. 2.1; in this scenario, the wetting/drying hysteresis is suppressed, because the system always follows the same sequence of states when pressure is varied. However, actual experiments (and simulations) have a finite duration, which may result in the system remaining trapped into local, metastable minima; in this case, wetting/drying hysteresis is expected. Its significances depend on the ratio between the experimental timescale and the one characterising the transition from the metastable to the stable state, Equation (11), which ensures equilibration. Starting from the free-energy profiles at different pressures (see Figure 4(c) for the case $\Delta P = 0$) and by inverting Equation (11) it is possible to predict the

conditions at which drying and wetting occur in cycles with prescribed frequency or duration (Figure 4(d)). These figures can be compared with the experimental ones measured in cycles of fixed duration [108], which are performed under the same conditions. It is seen that the drying pressure sensitively depends on the frequency of the cycles, while the dependence of the wetting pressure is not as pronounced [22]. This strong asymmetry is due to the different critical volumes characterising the two processes: very small for drying, which is related to the first asymmetric bubble spanning the entire pore diameter, while comparable in size to the entire pore for wetting (Figure 4(c)); Equation (12b) shows that this volume asymmetry is in turn reflected in large and small pressure differences required to change by the same amount the drying and wetting rates, respectively [21]. Overall, the hysteresis of the cycle decreases with frequency, because one tends to the thermodynamic limit where hysteresis is suppressed. Recent experimental work further considered the case in which defects in the hydrophobic coating are present within the nanopore, in which case the kinetics of drying in long pores may become dominated by the thermally activated jumping of the liquid front across surface defects [109].

In Sec. 2.2.1 (and typically in CNT) the effect of the geometry of confinement on drying kinetics is discussed based solely on the budget of bulk terms and positive and negative surface terms. At the nanoscale, however, where the effect of confinement on nucleation is more prominent, volume and surface terms may not be sufficient in order to describe the nucleation process. We have introduced already in Sec. 2.1 the more general free energy functional of morphometric thermodynamics, Equation (5), which includes two terms proportional to the integrated mean and Gaussian curvatures of each interface. These terms must be accounted for, assessing whether their contribution favours drying or not. In the presence of a third phase, an additional term τl_{tl} should be added, where τ is the tension of the triple line and l_{tl} its length [84,85]. Note that there is a conceptual difference between the line tension between three phases that are in thermodynamic equilibrium and that between two phases in equilibrium at a surface. The latter depends on the definition of the dividing interface, which is similar to the surface tension at a surface. Microscopic descriptions of the system, e.g. those provided by atomistic simulations, naturally encompass all these nanoscale effects which are encoded in the interactions among particles. Comparison of microscopic simulations/calculations with some sort of morphometric thermodynamics is particularly illuminating in that it allows to assess the relevance of these terms [20,21,110,111]. In particular, due to the difficulty to obtain experimental values, line tension has been the object of a number of recent simulation works [110,112]. In confinement, Debenedetti and coworkers [19] reported that a positive line tension was

needed in order to explain the simulated drying rates between two smooth plates facing each other at nanoscale distances (< 1.5 nm).

The increasing availability of high-resolution structural information on ion channels has allowed a burgeoning of molecular dynamics of ion channels [113]. The range of time scales and length scales accessible to atomistic simulations proved crucial to shed light on the microscopic mechanisms underlying, e.g. gating of ion channels. In particular, it was possible to prove that model [30] and realistic [31,34,36] ion channels show drying in the pore domain. Additional simulation efforts concern model pores which show the full generality of such drying phenomena [14,17,21,98].

In the following we review experimental, theoretical, and simulation results on drying in cylindrical nanopores, focusing on nanoscale effects. Recent experiments [22] on porous materials similar to Ref [42] were able to carefully measure the kinetics of drying in cylindrical, hydrophobic nanopores. Experiments at different temperatures clearly demonstrated the thermally activated signature of drying, typical of nucleation (cf. Equation (11)). Results were then interpreted in terms of the CNT of [42], finding that it predicted well the (almost constant) critical bubble volume but not the free-energy barriers, which were consistently lower than in the CNT prediction. The missing term was found to be a negative line tension $\tau \approx -20$ pN. Later, detailed atomistic simulations [21] were able to compute the free-energy profile (Figure 4(c)) and the drying mechanism on a hydrophobic cylinder with the same radius as the experiments. Such atomistic free-energy calculations allowed to compute the macroscopic and the atomistic free-energy profiles on the same drying path, solving the discontinuity problem of the CNT formulation. This comparison confirmed the crucial role of line tension in accelerating drying in nanoconfinement [21], with the estimate $\tau = -10$ pN.

Reference [21] also reported potential difficulties in interpreting porosimetry measurements for nanometre-scale pores; indeed, the usual procedure consists in estimating the pore radius or the contact angle from pressure measurements through Equation (4) using an independent measure of either θ_Y or R_c, respectively. However, consistently with Equation (8), the values taken by these two quantities depend on the choice of the dividing surface and on $\Delta\kappa$, both of which are not trivial to establish experimentally. Such nanoscale contributions are negligible for pores larger than some tens of diameters of the fluid particles (ca. 10 nm for a hydrophobic groove and a simple liquid [23], but the precise threshold depends on the confining geometry, on the nature of the liquid, etc.) but become significant when confinement increases. In DFT calculations or in MD simulations, on the other hand, it is possible to carefully define the position of the wall and to compute independently the Young contact angle; for example, using the centre of the wall atoms to define the pore radius and θ_Y computed on a flat wall, Ref [21] reported that the hydrophobicity inside cylindrical nanopores is effectively enhanced by the

nanoscale curvature. Rather than being a general rule, these results raise a caveat on interpreting experiments in nanopores in terms of θ_Y, R_c, and $\Delta\kappa$; the only well-defined quantity in this case seems ΔP.

3. Conclusions & perspectives

In this short review, we have analysed drying in extreme confinement, focusing especially on nanopores. A general framework for understanding the thermodynamics and the kinetics of this phenomenon has been outlined, clarifying how drying crucially depends on the size of confinement, on its hydrophobicity, and on its geometry. A general result is that the presence of hydrophobic surfaces favours drying, shifting towards higher hydrostatic pressures the conditions of vapour-liquid coexistence and accelerating drying kinetics. Decreasing the size and increasing the degree of confinement, e.g. going from grooves to pits, have analogous effects [27]. It is particularly pertinent the example of nanoscale cylindrical pores with hydrophobic walls immersed in water, which, at ambient temperature, undergo drying at hydrostatic pressures as large as tens of MPa [22,42], i.e. hundreds of MPa away from the bulk cavitation conditions [88].

Confined drying is central for a number of phenomena in biology and technology. In particular, we have discussed the hydrophobic gating mechanism in ion channels, in which the formation of nanoscale bubble blocks ionic currents [32]. Considering the typical size and hydrophobicity of ion channels, the physical mechanism of confined drying seems to apply to a number of them. Importantly, our discussion also highlighted that the random telegraph signal characteristic of single-channel currents is compatible with the typical kinetics of drying in nanometre confinement, provided that the conditions are close to coexistence between the dry and wet states. Although other indirect evidences of bubble gating have been reported [32], including many simulation ones [31,34–36], direct experimental evidence seems still elusive, due to the combination of small spatial scales and long timescales. In this context, theoretical predictions and detailed simulations may bridge structural information about proteins with functional measurements, such as electrophysiology, see, e.g. Ref [69]. As will be discussed below, much work is still to be done towards this end. On the technological side, drying in nanoporous materials was analysed in some detail. This case is doubly attractive because of the availability of accurate experimental data, which is useful for fostering theoretical understanding, and because of the technological interest of controlling wetting and drying of such materials which in turn determines their use as energy storage or dissipation devices [46]. The accumulated knowledge of drying in confinement can also be leveraged to control the wetting state of rough and textured hydrophobic surfaces, which is the key to realise robust superhydrophobic coatings. In

particular, nanoscale roughness can be exploited in order to achieve self-recovering superhydrophobic surfaces [27].

The present discussion highlights that several questions are still open in the field or have just started being asked. An important one is how drying is affected by complex environments, which is particularly relevant for biological examples. For instance, ion channels are proteins which enclose water [35]: this case encompasses both a chemically complex environment, with hydrophobic and hydrophilic interactions, and the elasticity inherent to proteins. In addition to structural complexity, in biological environments, ions are present in solution and non-equilibrium conditions may be relevant. While full-atom simulations of proteins account, at least partially, for such complexity, in order to achieve a physical understanding of the drying phenomena it is often fruitful to break down the problem in its different elements. In this latter direction, Debenedetti and coworkers investigated the effect of wall elasticity on drying between hydrophobic plates: it was found that elasticity always favoured water evaporation [114]. Non-equilibrium effects were studied in Ref [115]., where it was found that, while in the quasi-equilibrium picture wetting and drying happen along the same path, but in different directions, the dynamics of the transition may lead to qualitatively different mechanisms, which strongly depend on pressure. It has also been reported that dissolved gases, in particular low-solubility ones, may favour drying of nanopores [14,32]; this kind of gas-assisted drying calls for further investigations, as it may play an important role in general anaesthetics [32], in controlling drying of nanoporous materials and superhydrophobic surfaces, and in the stability of surface nanobubbles [97].

In conclusion, we have selectively reviewed the current status of theory, experiments, and simulations of drying in nanopores with the intent of achieving a coherent picture of the underlying physics. The interest of these phenomena is strongly crossdisciplinary, being of importance in biology, medicine, material science, and engineering. In particular, we have discussed the case of hydrophobic gating in ion channels and drying in hydrophobic nanoporous materials. The available results suggest that the size, the hydrophobicity, and the degree of confinement concur to promote the evaporation of water in nanopores; actually, the consequences are much more general and concern different liquids, provided that the relevant thermodynamic parameters, in primis solvophobicity, are correctly mapped. We further discussed nanoscale effects in drying, including the importance of line tension, and the open questions in the field, which call for a renewed synergistic research effort combining experiments, theory, and simulations.

Notes

1. This is not the only mechanism by which ion permeation can blocked; in general, in order to be able to pass through a pore – be it an ion channel or an artificial membrane – the ion should carry its full solvation shell [116]. Accordingly, drying of the pore further increases the barrier to ion permeation, leading to rejection of ions even when the pore radius alone would suggest an open state [34].

2. The grand canonical ensemble is defined as having constant chemical potential μ, volume V, and temperature T. The relevant thermodynamic potential is the grand canonical potential. This is the most convenient ensemble for discussing wetting and drying phenomena [71,117] and will be used in all our derivations; however, we will generically refer to 'free energy' to underscore that other ensembles and thermodynamic potentials could be used.

ORCID

Alberto Giacomello http://orcid.org/0000-0003-2735-6982
Roland Roth http://orcid.org/0000-0001-6271-7646

References

[1] Arndt REA. Cavitation in fluid machinery and hydraulic structures. Annu Rev Fluid Mech. 1981;13:273–328.

[2] Acosta AJ, Parkin BR. Cavitation inception - a selective review. J Ship Res. 1975;19:193–205.

[3] Crum LA. Tensile strength of water. Nature. 1979;278:148–149.

[4] Huang DM, Chandler D. Temperature and length scale dependence of hydrophobic effects and their possible implications for protein folding. Proc Natl Acad Sci USA. 2000;97:8324–8327.

[5] Huang X, Margulis CJ, Berne BJ. Dewetting-induced collapse of hydrophobic particles. Proc Natl Acad Sci USA. 2003;100:11953–11958.

[6] Giovambattista N, Lopez CF, Rossky PJ, et al. Hydrophobicity of protein surfaces: separating geometry from chemistry. Proc Natl Acad Sci USA. 2008;105:2274–2279.

[7] Berne BJ, Weeks JD, Zhou R. Dewetting and hydrophobic interaction in physical and biological systems. Annu Rev Phys Chem. 2009;60:85–103.

[8] Miller TF, Vanden-Eijnden E, Chandler D. Solvent coarse-graining and the string method applied to the hydrophobic collapse of a hydrated chain. Proc Natl Acad Sci USA. 2007;104:14559–14564.

[9] Mondal J, Morrone JA, Berne B. How hydrophobic drying forces impact the kinetics of molecular recognition. Proc Natl Acad Sci USA. 2013;110:13277–13282.

[10] Tanford C. The hydrophobic effect and the organization of living matter. Science. 1978;200:1012–1018.

[11] Chandler D. Interfaces and the driving force of hydrophobic assembly. Nature. 2005;437:640–647.

[12] Lum K, Chandler D, Weeks JD. Hydrophobicity at small and large length scales. J Phys Chem B. 1999;103:4570–4577.

[13] Talanquer V, Oxtoby D. Nucleation in a slit pore. J Chem Phys. 2001;114:2793–2801.

[14] Leung K, Luzar A, Bratko D. Dynamics of capillary drying in water. Phys Rev Lett. 2003;90:065502.

[15] Allen R, Hansen JP, Melchionna S. Molecular dynamics investigation of water permeation through nanopores. J Chem Phys. 2003;119:3905–3919.

[16] Vishnyakov A, Neimark AV. Nucleation of liquid bridges and bubbles in nanoscale capillaries. J Chem Phys. 2003;119:9755–9764.

[17] Desgranges C, Delhommelle J. Free energy calculations along entropic pathways. iii. nucleation of capillary bridges and bubbles. J Chem Phys. 2017;146:184104.

[18] Husowitz B, Talanquer V. Nucleation in cylindrical capillaries. J Chem Phys. 2004;121:8021–8028.

[19] Sharma S, Debenedetti PG. Evaporation rate of water in hydrophobic confinement. Proc Natl Acad Sci USA. 2012;109:4365–4370.

[20] Remsing RC, Xi E, Vembanur S, et al. Pathways to dewetting in hydrophobic confinement. Proc Natl Acad Sci USA. 2015;112:8181–8186.

[21] Tinti A, Giacomello A, Grosu Y, et al. Intrusion and extrusion of water in hydrophobic nanopores. Proc Natl Acad Sci USA. 2017;114:E10266–E10273.

[22] Guillemot L, Biben T, Galarneau A, et al. Activated drying in hydrophobic nanopores and the line tension of water. Proc Natl Acad Sci USA. 2012;109:19557–19562.

[23] Giacomello A, Schimmele L, Dietrich S, et al. Perpetual superhydrophobicity. Soft Matter. 2016;12:8927–8934.

[24] Prakash S, Xi E, Patel AJ. Spontaneous recovery of superhydrophobicity on nanotextured surfaces. Proc Natl Acad Sci USA. 2016;113:5508–5513.

[25] Li Y, Quéré D, Lv C, et al. Monostable superrepellent materials. Proc Natl Acad Sci USA. 2017 mar;114:3387–3392.

[26] Lisi E, Amabili M, Meloni S, et al. Self-recovery superhydrophobic surfaces: modular design. ACS Nano. 2018;12:359–367.

[27] Giacomello A, Schimmele L, Dietrich S, et al. Recovering superhydrophobicity in nanoscale and macroscale surface textures. Soft Matter. 2019;15:7462–7471.

[28] Hille B. Ionic channels of excitable membranes. Second edition. Sunderland, Massachusetts, USA: Sinauer Associates, Inc.; 1991.

[29] Beckstein O, Biggin PC, Sansom MS. A hydrophobic gating mechanism for nanopores. J Phys Chem B. 2001;105:12902–12905.

[30] Beckstein O, Sansom MS. Liquid–vapor oscillations of water in hydrophobic nanopores. Proc Natl Acad Sci USA. 2003;100:7063–7068.

[31] Anishkin A, Sukharev S. Water dynamics and dewetting transitions in the small mechanosensitive channel MscS. Biophys J. 2004;86:2883–2895.

[32] Roth R, Gillespie D, Nonner W, et al. Bubbles, gating, and anesthetics in ion channels. Biophys J. 2008;94:4282–4298.

[33] Anishkin A, Akitake B, Kamaraju K, et al. Hydration properties of mechanosensitive channel pores define the energetics of gating. J Phys: Condens Matter. 2010;22:454120.

[34] Zhu F, Hummer G. Drying transition in the hydrophobic gate of the GLIC channel blocks ion conduction. Biophys J. 2012;103:219–227.

[35] Aryal P, Sansom MS, Tucker SJ. Hydrophobic gating in ion channels. J Mol Biol. 2015;427:121–130.

[36] Rao S, Lynch CI, Klesse G, et al. Water and hydrophobic gates in ion channels and nanopores. Faraday Discuss. 2018;209:231–247.

[37] Heimburg T. Lipid ion channels. Biophys Chem. 2010;150:2–22.

[38] Blicher A, Heimburg T. Voltage-gated lipid ion channels. PLoS One. 2013;8:e65707.

[39] Bayley H, Braha O, Kasianowicz J, et al. Designed protein pores as components for biosensors. US Patent App. 10/946,802. 2005.

[40] Stoddart D, Heron AJ, Mikhailova E, et al. Single-nucleotide discrimination in immobilized DNA oligonucleotides with a biological nanopore. Proc Natl Acad Sci USA. 2009;106:7702–7707.

[41] Huang G, Voet A, Maglia G. Frac nanopores with adjustable diameter identify the mass of opposite-charge peptides with 44 dalton resolution. Nat Comm. 2019;10:1–10.

[42] Lefevre B, Saugey A, Barrat JL, et al. Intrusion and extrusion of water in hydrophobic mesopores. J Chem Phys. 2004;120:4927–4938.

[43] Han A, Kong X, Qiao Y. Pressure induced liquid infiltration in nanopores. J Appl Phys. 2006;100:014308.

[44] Smirnov S, Vlassiouk I, Takmakov P, et al. Water confinement in hydrophobic nanopores. pressure-induced wetting and drying. ACS Nano. 2010;4:5069–5075.

[45] Amabili M, Grosu Y, Giacomello A, et al. Pore morphology determines spontaneous liquid extrusion from nanopores. ACS Nano. 2019;13:1728–1738.

[46] Eroshenko V, Regis RC, Soulard M, et al. Energetics: a new field of applications for hydrophobic zeolites. J Am Chem Soc. 2001;123:8129–8130.

[47] Eroshenko V, Regis RC, Soulard M, et al. The heterogeneous systems 'water-hydrophobic zeolites': new molecular springs. C R Phys. 2002;3:111–119.

[48] Nagashima G, Levine EV, Hoogerheide DP, et al. Superheating and homogeneous single bubble nucleation in a solid-state nanopore. Phys Rev Lett. 2014;113:024506.

[49] Eroshenko V. Heterogeneous structure for accumulating or dissipating energy, methods of using such a structure and associated devices. US Patent 6,052,992. 2000.

[50] Eroshenko V, Piatiletov I, Coiffard L, et al. A new paradigm of mechanical energy dissipation. part 2: experimental investigation and effectiveness of a novel car damper. Proc Inst Mech Eng Part D. 2007;221:301–312.

[51] Iwatsubo T, Suciu CV, Ikenagao M, et al. Dynamic characteristics of a new damping element based on surface extension principle in nanopore. J Sound Vib. 2007;308:579–590.

[52] Rauscher M, Dietrich S. Wetting phenomena in nanofluidics. Annu Rev Mater Res. 2008;38:143–172.

[53] Sachs F, Qin F. Gated, ion-selective channels observed with patch pipettes in the absence of membranes: novel properties of a gigaseal. Biophys J. 1993;65:1101–1107.

[54] Smeets RM, Keyser U, Wu M, et al. Nanobubbles in solid-state nanopores. Phys Rev Lett. 2006;97:088101.

[55] Smeets RM, Keyser UF, Dekker NH, et al. Noise in solid-state nanopores. Proc Natl Acad Sci USA. 2008;105:417–421.

[56] Smirnov SN, Vlassiouk IV, Lavrik NV. Voltage-gated hydrophobic nanopores. ACS Nano. 2011;5:7453–7461.

[57] Polster JW, Acar ET, Aydin F, et al. Gating of hydrophobic nanopores with large anions. ACS Nano. 2020;14:4306–4315.

[58] Powell MR, Cleary L, Davenport M, et al. Electric-field-induced wetting and dewetting in single hydrophobic nanopores. Nat Nanotech. 2011;6:798.

[59] Marion S, Macha M, Davis SJ, et al. Wetting of nanopores probed with pressure. arXiv. 2019;1911.05229v2. https://arxiv.org/abs/1911.05229v2.

[60] Lee J, Karnik R. Desalination of water by vapor-phase transport through hydrophobic nanopores. J Appl Phys. 2010;108:044315.

[61] Lee J, Laoui T, Karnik R. Nanofluidic transport governed by the liquid/vapour interface. Nat Nanotechnol. 2014;9:317–323.

[62] Duan C, Karnik R, Lu MC, et al. Evaporation-induced cavitation in nanofluidic channels. Proc Natl Acad Sci USA. 2012;109:3688–3693.

[63] Hummer G, Rasaiah JC, Noworyta JP. Water conduction through the hydrophobic channel of a carbon nanotube. Nature. 2001;414:188–190.

[64] Checco A, Ocko BM, Rahman A, et al. Collapse and reversibility of the superhydrophobic state on nanotextured surfaces. Phys Rev Lett. 2014;112:216101.

[65] Helmy R, Kazakevich Y, Ni C, et al. Wetting in hydrophobic nanochannels: a challenge of classical capillarity. J Am Chem Soc. 2005;127:12446–12447.

[66] Doyle DA, Cabral JM, Pfuetzner RA, et al. The structure of the potassium channel: molecular basis of K+ conduction and selectivity. Science. 1998;280:69–77.

[67] Hamill OP, Marty A, Neher E, et al. Improved patch-clamp techniques for high-resolution current recording from cells and cell-free membrane patches. Pflügers Archiv. 1981;391:85–100.

[68] Neher E, Sakmann B. Single-channel currents recorded from membrane of denervated frog muscle fibres. Nature. 1976;260:799–802.

[69] Dror RO, Dirks RM, Grossman J, et al. Biomolecular simulation: a computational microscope for molecular biology. Annu Rev Biophys. 2012;41:429–452.

[70] Evans R, Marconi UMB, Tarazona P. Fluids in narrow pores: adsorption, capillary condensation, and critical points. J Chem Phys. 1986;84:2376–2399.

[71] Dietrich S. Wetting phenomena. In: Domb C, Lebowitz JL, editors. Phase transitions and critical phenomena. Vol. 12, Chapter 1. London: Academic Press; 1988. p. 1–218.

[72] Rascón C, Parry A. Geometry-dominated fluid adsorption on sculpted solid substrates. Nature. 2000;407:986.

[73] Restagno F, Bocquet L, Biben T. Metastability and nucleation in capillary condensation. Phys Rev Lett. 2000;84:2433.

[74] Yatsyshin P, Savva N, Kalliadasis S. Wetting of prototypical one-and two-dimensional systems: thermodynamics and density functional theory. J Chem Phys. 2015;142:034708.

[75] Lafuma A, Quéré D. Superhydrophobic states. Nat Mater. 2003;2:457–460.

[76] Quéré D. Wetting and roughness. Annu Rev Mater Res. 2008;38:71–99.

[77] Evans R. Fluids adsorbed in narrow pores: phase equilibria and structure. J Phys: Condens Matter. 1990;2:8989–9007.

[78] König PM, Roth R, Mecke KR. Morphological thermodynamics of fluids: shape dependence of free energies. Phys Rev Lett. 2004;93:160601–1–4.

[79] Hardwiger H. Vorlesungen über Inhalt, Oberfläche und Isoperimetrie. Berlin, Göttingen, Heidelberg: Springer; 1957.

[80] Roth R, Kroll KM. Capillary evaporation in pores. J Phys: Condens Matter. 2006;18:6517–6530.

[81] Peyser A, Gillespie D, Roth R, et al. Domain and interdomain energetics underlying gating in shaker-type K_V channels. Biophys J. 2014;107:1841–1852.

[82] Gußmann F, Roth R. Bubble gating in biological ion channels: a density functional theory study. Phys Rev E. 2017;95:062407–1–7.

[83] Thompson AN, Posson DJ, Parsa PV, et al. Molecular mechanism of pH sensing in KcsA potassium channels. Proc Natl Acad Sci USA. 2008;105:6900–6905.

[84] Rowlinson JS, Widom B. Molecular theory of capillarity. Oxford: Oxford University Press; 1982.

[85] Schimmele L, Napiórkowski M, Dietrich S. Conceptual aspects of line tensions. J Chem Phys. 2007;127:164715.

[86] Skripov VP. Metastable liquids. New York: Halsted Press; 1972.

[87] Volmer, M. Kinetik der Phasenbildung. Dresden und Leipzig: Steinkopff. In: Steinkopff T, editor. Kinetik der Phasenbildung; 1939.

[88] Caupin F, Herbert E. Cavitation in water: a review. C R Phys. 2006;7:1000–1017.

[89] Meloni S, Giacomello A, Casciola CM. Focus article: theoretical aspects of vapor/gas nucleation at structured surfaces. J Chem Phys. 2016;145:211802.

[90] Giacomello A, Chinappi M, Meloni S, et al. Metastable wetting on superhydrophobic surfaces: continuum and atomistic views of the Cassie-Baxter–Wenzel transition. Phys Rev Lett. 2012;109:226102.

[91] Giacomello A, Chinappi M, Meloni S, et al. Geometry as a catalyst: how vapor cavities nucleate from defects. Langmuir. 2013;29:14873–14884.

[92] Zheng Q, Durben D, Wolf G, et al. Liquids at large negative pressures: water at the homogeneous nucleation limit. Science. 1991;254:829–832.

[93] Azouzi MEM, Ramboz C, Lenain JF, et al. A coherent picture of water at extreme negative pressure. Nat Phys. 2013;9:38–41.

[94] Atchley AA, Prosperetti A. The crevice model of bubble nucleation. J Acoust Soc Am. 1989;86:1065–1084.

[95] Gritti, F, Brousmiche, D, Gilar, M, Walter, TH, Wyndham, K. Kinetic mechanism of water dewetting from hydrophobic stationary phases utilized in liquid chromatography. *J Chromatogr A*. 2019;1596, 41–53. doi:10.1016/j.chroma.2019.02.051

[96] Bakalyar S, Bradley MT, Honganen R. The role of dissolved gases in high-performance liquid chromatography. J Chromatogr A. 1978;158:277–293.

[97] Tortora M, Meloni S, Tan BH, et al. The interplay among gas, liquid and solid interactions determines the stability of surface nanobubbles; 2020.

[98] Luzar A. Activation barrier scaling for the spontaneous evaporation of confined water. J Phys Chem B. 2004;108:19859–19866.

[99] Roth R, Parry AO. Drying in a capped capillary. Mol Phys. 2011;109:1159–1167.

[100] Roth R, Parry AO. Geometrical aspects of drying in a capped capillary: a DFT Study. J Phys Soc Jpn. 2012;81:SA009.

[101] Rejmer K, Dietrich S, Napiórkowski M. Filling transition for a wedge. Phys Rev E. 1999;60:4027–4042.

[102] Grosu Y, Li M, Peng YL, et al. A highly stable nonhysteretic {Cu_2(tebpz) MOF+water} molecular spring. ChemPhysChem. 2016;17:3359–3364.

[103] Giacomello A, Schimmele L, Dietrich S. Wetting hysteresis induced by nanodefects. Proc Natl Acad Sci USA. 2016;113:E262–E271.

[104] Bussonnière A, Liu Q, Tsai PA. Cavitation nuclei regeneration in a water-particle suspension. Phys Rev Lett. 2020;124:034501.

[105] Giacomello A, Meloni S, Müller M, et al. Mechanism of the Cassie-Wenzel transition via the atomistic and continuum string methods. J Chem Phys. 2015;142:104701.

[106] Amabili M, Meloni S, Giacomello A, et al. Activated wetting of nanostructured surfaces: reaction coordinates, finite size effects, and simulation pitfalls. J Phys Chem B. 2018;122:200–212.

[107] Tinti A, Giacomello A, Casciola CM. Vapor nucleation paths in lyophobic nanopores. Eur Phys J E. 2018;41:52.

[108] Guillemot L, Galarneau A, Vigier G, et al. New device to measure dynamic intrusion/extrusion cycles of lyophobic heterogeneous systems. Rev Sci Instrum. 2012;83:105105.

[109] Michel L Etude macroscopique dynamique et microscopique des systèmes hétérogènes lyophobes [dissertation]. Université Grenoble Alpes; 2019.

[110] Weijs JH, Marchand A, Andreotti B, et al. Origin of line tension for a Lennard-Jones nanodroplet. Phys Fluids. 2011;23:022001.

[111] Amabili M, Giacomello A, Meloni S, et al. Collapse of superhydrophobicity on nanopillared surfaces. Phy Rev Fluids. 2017;2:034202.

[112] Kanduč M. Going beyond the standard line tension: size-dependent contact angles of water nanodroplets. J Chem Phys. 2017;147:174701.

[113] Flood E, Boiteux C, Lev B, et al. Atomistic simulations of membrane ion channel conduction, gating, and modulation. Chem Rev. 2019;119:7737–7832.

[114] Altabet YE, Haji-Akbari A, Debenedetti PG. Effect of material flexibility on the thermodynamics and kinetics of hydrophobically induced evaporation of water. Proc Natl Acad Sci USA. 2017;114:E2548–E2555.

[115] Marchio S, Meloni S, Giacomello A, et al. Wetting and recovery of nano-patterned surfaces beyond the classical picture. Nanoscale. 2019;11:21458–21470.

[116] Beckstein O, Tai K, Sansom MS. Not ions alone: barriers to ion permeation in nanopores and channels. J Am Chem Soc. 2004;126:14694–14695.

[117] Evans R. The nature of the liquid-vapour interface and other topics in the statistical mechanics of non-uniform, classical fluids. Adv Phys. 1979;28:143–200.